

Micro Optical Components Fabrication by Laser Processing

Narayana Raju Gottumukkala

Department of Electrical and Computer Engineering

University of Virginia

December 2021

A thesis submitted to the faculty of Graduate Studies in partial fulfillment of the degree Masters of Engineering

Abstract

Micro-optical components – like lenses, diffraction gratings, and photon sieves find many applications in optoelectronics devices such as display, scanners, imaging, and information storage. In this thesis, we describe the design, fabrication and characterization of the micro-optical components fabricated by laser processing method and using Zemax ray-tracing simulations, measurement of optical beam profile, surface morphology and optical transmission efficiencies.

Plano-concave micro lenses were fabricated using a 355 nm wavelength pulsed picosecond laser and CW CO₂ lasers. The plano-convex lenses were fabricated by picosecond laser micro patterning followed by reshaping the patterned area using a CO₂ laser melting. Plano-concave, plano-convex and cylindrical lenses were fabricated, and their performance in terms of light transmission efficiency, focal length, and beam divergences was characterized. A comparative study of the micro lenses fabricated by different technique was also carried out.

Diffraction gratings were micro machined of about 10 μm period in sapphire using a 355 nm wavelength nanosecond pulsed laser and high NA objective lens. The fabricated gratings were characterized in terms of diffracted beam profile, optical diffraction efficiency, surface morphology, and depth profile of gratings when the laser was focused on the top surface and also at the bottom surface of the sapphire sample. We also demonstrate the fabrication of a photon sieve, a planar diffractive optical lens based on diffraction phenomenon on a sapphire substrate for operation at 632 nm wavelength, and characterized the output beam profile of the focused beam.

Microscale (200μm) glass sealing was achieved using a 1070 nm wavelength CW laser by melting glass frit between glass plates at room temperature. The optical transmission and strength of the glass bond was investigated and compared to the conventional furnace glass sealing process.

In summary, improved methods to fabricate micro-optical components with low cost, large area, and low process times have been demonstrated with laser processing.

Acknowledgments

I would like to express my sincere gratitude to my advisor, Prof. Mool C. Gupta, for providing the opportunity and support for my masters degree program and thesis research. His patience, passion for research, and supportive mentoring will be incredibly valuable in my future research and career life. I would also like to convey my gratitude to my committee members, Prof. Andreas Beling and Prof. Kyusang Lee, for the insightful comments and suggestions in the dissertation process.

I would like to thank my colleagues in Prof. Gupta's research group. Dr. George Wilkes, Dr. Ahmed Rasin, Arpan Sinha, Joel Harrison, Dr. Chris Duska, Md Toriqul Islam, Elisa Pantoja, and Dr. Alan Mulronev for their friendship and assistance in my research.

This Thesis was supported by the NASA Langley professor program and partially supported by Corning Inc. Thanks to Nanoscale Materials Characterization Facility (NMCF) and UVML facility members, Richard White, and Catherine A. Dukes. Thanks to the ECE staff, Crystal Aldridge, and Beth Eastwood-Beatty.

List of Figures

Figure 1: Picosecond laser setup.	5
Figure 2: CO ₂ laser experiment setup.	6
Figure 3: UV nanosecond pulsed laser setup.	7
Figure 4: Schematic of the laser glass sealing process.....	8
Figure 5: Direction of laser scanning.	8
Figure 6: IR laser setup with heatsink.	8
Figure 7: Beam profile measurement setup.....	9
Figure 8: Quantitative adhesion test setup.	9
Figure 9: SEM image of concave MLAs using CO ₂ laser. (A) Individual concave lenses. (B) Concave lenses with random overlap.	10
Figure 10: Simulated beam profile of Gaussian beam after passing through the CO ₂ fabricated concave MLA at various distances from the lens (A) 5 mm, and (B) 10 mm. Experimentally measured beam profile after passing through the CO ₂ concave MLA at various distances from the lens (C) 5 mm, and (D) 10 mm.	11
Figure 11: SEM image of concave MLAs using picosecond laser. (A) Individual concave lens. (B) Concave lenses with random overlap.	12
Figure 12: Simulated beam profile of Gaussian beam after passing through the picosecond laser fabricated concave MLA at various distances from the lens (A) 5 mm, and (B) 10 mm. Experimentally measured beam profile after passing through the picosecond laser fabricated concave MLA at various distances from the lens (C) 5 mm, and (D) 10 mm.	13
Figure 13: SEM image of (A) picosecond laser micromachined line pattern. (B) cylindrical lenses after CO ₂ laser melting.	14
Figure 14: Simulated beam profile of Gaussian beam after passing through the cylindrical MLA at various distances from the lens (A) 5 mm, and (B) 10 mm. Experimentally measured beam profile after passing through the cylindrical MLA at various distances from the lens (C) 5 mm, and (D) 10 mm.	15

Figure 15: SEM image of (A) picosecond laser micromachined perpendicular line pattern. (B) convex lenses after CO ₂ laser melting.....	16
Figure 16: Simulated beam profile of Gaussian beam after passing through the convex MLA at various distances from the lens (A) 5 mm, (B) 10 mm, and (C) flat top beam profile after beam passes through MLA and convex lens. Experimentally measured beam profile after passing through the convex MLA at various distances from the lens (D) 5 mm, (E) 10 mm, (F) flat top beam profile after beam passes through MLA and convex lens.....	17
Figure 17: SEM image of diffraction grating pattern when laser beam was focused on the top surface.	19
Figure 18: Diffraction grating beam profile for pattern fabrication on the top surface.	19
Figure 19: SEM image of diffraction grating pattern when laser beam was focused on the bottom surface.....	20
Figure 20: Diffraction grating beam profile for pattern fabrication on the bottom surface.	20
Figure 21: SEM image of photon sieve on sapphire substrate.....	21
Figure 22: Experimentally measured beam profile (A)He-Ne laser, (B) after passing through the photon sieve, 77 mm from the photon sieve surface.....	21
Figure 23: Temperature cycle for glass furnace melting.....	22
Figure 24: Optical Transmission measurement for (a)TEST A and (b)TEST b.	23
Figure 25: Optical image of laser melted glass frit for (A) furnace melted glass frit and (B) TEST B sample.....	24
Figure 26: Seal strength measurements for (a)TEST A and (b)TEST B.	25

List of Tables

Table 1. Comparison of lens parameter for various fabrication processes. 18

List of Symbols, Abbreviations, and Acronyms

3D	3 dimensional
CO ₂	carbon dioxide
CMOS	complementary metal oxide semiconductor
CTE	coefficient of thermal expansion
CW	continuous wave
DOE	diffractive optical elements
FWHM	full width half maximum
IPA	isopropyl alcohol
QCW	quasi-continuous wave
MLA	micro-lens array
NA	numerical aperture
NIR	near infrared
LED	light emitting diodes
OLED	organic light emitting diodes
OSC	organic solar cells
SEM	scanning electron microscope
T _g	glass transition temperature
UV	ultraviolet
Vis	visible light
W	watts

Table of Contents

Abstract	ii
Acknowledgments	iv
List of Figures	v
List of Tables.....	vii
List of Symbols, Abbreviations, and Acronyms	viii
Table of Contents	ix
1. Introduction	1
1.1 Micro-lens array	1
1.2 Laser micro-scale processing of sapphire for diffraction gratings and photon sieve.....	2
1.3 Micro sealing of glass	3
2. Experimental	5
2.1 Fabrication.....	5
2.1.1 Micro lens array fabrication.....	5
2.1.2 Laser micro patterning of sapphire	6
2.1.3 Laser-assisted micro-glass vacuum sealing	7
2.2 Characterization	9
3. Results	10
3.1 Micro lens array properties	10
3.1.1 Concave lens fabrication by CO ₂ laser	10
3.1.2 Concave lens fabrication by picosecond laser	12
3.1.3 Cylindrical lens fabrication by combining picosecond and CO ₂ lasers.....	13
3.1.4 Convex lens fabrication by combining CO ₂ and picosecond laser	15
3.2 Laser micro patterning of sapphire	18
3.2.1 Fabrication of Diffraction gratings	18
3.2.2 Fabrication of photon sieve.....	20
3.3 Micro scale laser-assisted glass vacuum sealing.....	22

4.	Conclusions and Future Work.....	26
4.1	Conclusions	26
4.2	Future Work	27
4.2.1	Micro-lens	27
4.2.2	Micro-patterning	27
	Appendix: Publications	28
A.	Fabrication and Comparative Study of Micro-Lenses Obtained by Solid State Pico-Second and CW CO ₂ Laser.	28
B.	Fabrication and Optical Analysis of Diffractive Optical Elements by Nanosecond Pulsed Laser	29
C.	Glass Sealing by CW Laser Melting of Low Temperature Frit	30
	References	31

1. Introduction

As imaging systems are getting extremely miniaturized, the need for high-efficiency micro-optical elements is growing. This has drawn a lot of attention from researchers in various fields to find new techniques to fabricate micro-optical elements such as micro lenses, diffraction gratings, photon sieves, and micro scale hermetic sealing for optoelectronic applications. Recently, high-power lasers have been used for the fabrication of micro-optical elements on optically transparent materials such as fused silica, sapphire, and borosilicate glass. Lasers can provide high temperatures at localized regions for the short-pulsed duration for surface patterning or in continuous wave (CW) mode to melt glass.

1.1 Micro-lens array

Micro-lens arrays (MLAs) consist of many miniature lenses, like an insect compound eye. They have lower image resolution and sensitivity than macro lenses, so they are more suitable for fiber coupling homogenizers, laser beam shaping, light field cameras, LED light management, 3D integral imaging, and increasing efficiency in photovoltaics. Due to broad applications, several MLA fabrication techniques have been developed, such as photolithography, surface tension-based curing, direct laser writing, thermal reflow, and embossing. MLAs can be either plano-concave or plano-convex lenses. Concave MLAs have previously been obtained using femtosecond laser pulses on fused silica followed by hydrofluoric acid etching [1][2], but this process takes 50 minutes to form concave lenses for 1 in². Convex MLAs are less commonly produced with laser techniques but have broader applications. Direct laser writing [3], can obtain convex lens but they still suffer from 60 minute process times for 1 in². Thermal reflow and micro nozzle printing [4][5] use photoresist, UV curable polymers, and other low-temperature materials

to develop a convex lens. Template mold imprinting [6] uses masks and ball end mill to form a lens that adds process steps, and the CMOS compatible process [7] and can generate high-quality micro lenses but add fabrication costs and process time.

In this thesis, we describe a process for concave lens formation using a pulsed picosecond laser and a CO₂ laser as well as that uses a picosecond laser for surface patterning and a CO₂ laser to reflow the fused silica to form convex lenses. The described process eliminates masks and wet chemical etching. This fabrication process provides MLAs with high light transmission efficiency, cost-effectiveness, and process times as low as a few minutes for 1 in² area. We also provide a comparative study of the lens formed using individual CO₂ and UV picosecond lasers and compare surface morphology, surface profile, and beam characteristics with simulations.

The scientific studies have included MLAs fabricated using pulsed and CW CO₂ lasers, picosecond laser [8], femtosecond laser and CO₂ laser [9], short-pulsed CO₂ laser [10], for the fabrication of beam homogenizers [11], and cylindrical micro lens [12]. All of the previous studies lack a comparative performance analysis between pulsed and CW lasers. In this study, fabricating micro lenses by picosecond and CO₂ laser and combining picosecond micromachining with CO₂ melting allows us to perform a detailed performance comparison study of various types of lasers fabricated convex and concave micro lenses reported in the literature.

1.2 Laser micro-scale processing of sapphire for diffraction gratings and photon sieve

Diffraction optical elements (DOEs) such as gratings and photon sieves provide a planar alternative to traditional refractive lenses. DOEs operate on the principle of optical diffraction and interference. The diffractive property provides improved chromatic aberration reduction for a large wavelength spectrum. Many applications like space telescopes [13], imaging systems [14], fiber waveguide coupling[15], and optical interconnects [16] can use diffractive optical elements.

Fabrication of DOEs is commonly done by lithography [17] but, this adds multiple process steps involving masks, increasing costs, and is typically a very slow process.

Micromachining by lasers will eliminate all of the process steps like photoresist, chemical etching, mask fabrication and provide large-area processing, and lowers the cost significantly. High power and short pulse width lasers [18][19] have been used for material surface patterning. Using higher NA objectives, the feature sizes in the order of hundred nanometers to tens of microns have been achieved [20].

Photon sieves are designed similar to Fresnel zone plates where the zones consist of circular pin holes. Compared to zone plate optics, photon sieves provide focal points with high suppression of higher order maxima [21]. Photon sieves can be designed for certain wavelength [22] and the focal position can be controlled by changing the pin hole diameter and pin hole distribution.

In this thesis, we describe the process of micromachining sapphire using UV nanosecond pulsed laser, and provide data on surface morphology, beam profiles for diffraction gratings and photon sieve. We also compare the results when the direct laser ablation is performed on the top surface and on the bottom surface, when the laser passing the sapphire material.

1.3 Micro sealing of glass

Hermetic encapsulation is a primary requirement for components and devices such as energy-efficient windows, OLED displays, and organic solar cells (OSC). Generally, any device or material that degrades due to interaction with the external environment over time (i.e., oxidation or moisture) would benefit from hermetic sealing. Laser sintering of glass frit for sealing glass plates has shown to be a more efficient process [23][24] [25]. The amount of thermal energy used

and processing time for laser sintering is a fraction of the conventional furnace process [26]. Glass frits are generally produced in the form of glass pastes, which are a mixture of glass powder and solvents, binders, or fillers. Using different oxides, the coefficient of thermal expansion (CTE) and transition temperature (T_g) of the frit can be controlled. The localized melting from laser radiation should generate enough thermal energy to reach the glass transition temperature and create a melt pool for glass bonding.

Laser-assisted glass frit bonding has been reported by several researchers, Emami S. [23] work was on soda-lime glass bonding using CW laser of wavelength 1070 nm with process temperature of 120 °C. For devices that cannot withstand high processing temperatures, Lorenz N. [27] reported bonding in air and vacuum using a 200 W CW laser of wavelength 940 nm and preheating treatment of the glass frit. Logunov [28] work was on multiple glass types that were bonded using 30 W CW laser of wavelength of 810 nm and CW laser power of 400 W of wavelength 940 nm. Logunov reported results on stress measurements and the effect on bond quality due to laser spot size, glass thickness, and sealing speed. Similarly, Fernando R. [25] and Ivanou D K. [29] work was on glass frit sealing for dye-sensitized solar cells.

Usually, an external heating source is used to reduce thermal shocks in the glass substrates during localized laser irradiation. The lack of uniform thermal stress can lead to cracks, delamination, and failures in the seal between glass plates. Also, glass plates themselves can crack. Borosilicate glass is desirable for large-scale applications as well as could eliminate the need for preheating and hence is the main focus of this study.

2. Experimental

2.1 Fabrication

2.1.1 Micro lens array fabrication

A 355 nm wavelength picosecond laser was used to inscribe arrays on fused silica. The UV picosecond laser was a Spectra-Physics IceFyre 355-30, operated at 350 kHz pulse repetition rate, 30 W average power, and 10 ps pulse width shown in figure 1. The laser beam was directed using the Sino-Galvo SG7210 system. The sample inscribing velocity was set to 1000 mm/s. The CO₂ laser was used for both to form lens arrays or remelt fused silica after the picosecond laser. The CO₂ laser was Senfeng SF1390i which is a continuous wave (CW) laser with 150 W average power and 300 μm spot size, shown in figure 2. A Newmark e-track XY stage with 100 mm/s speed was used to form MLA on the fused silica.

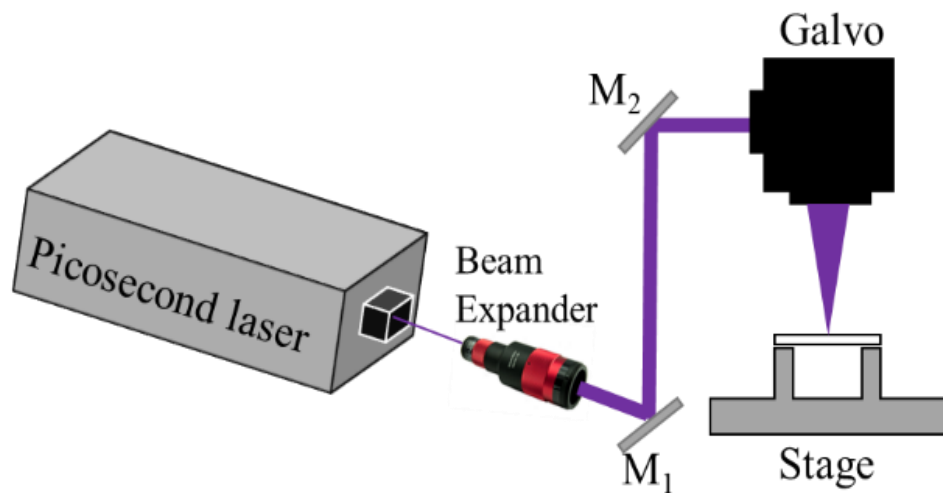


Figure 1: Picosecond laser setup.

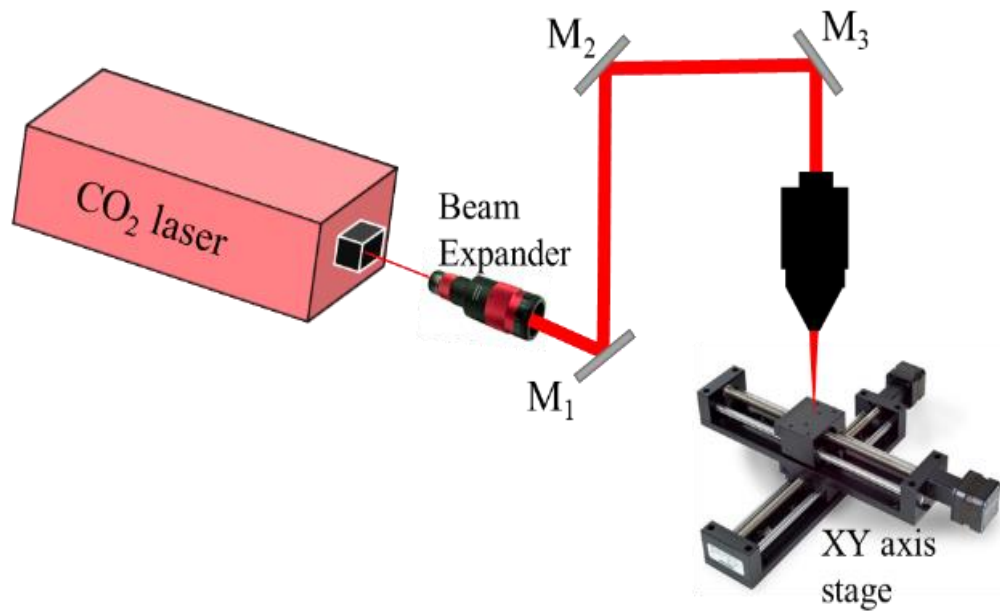


Figure 2: CO₂ laser experiment setup.

2.1.2 Laser micro patterning of sapphire

A 355 nm wavelength nanosecond pulsed laser was used to inscribe arrays on sapphire. The UV nanosecond laser was a Coherent Matrix 355-8-50, operated at 30 kHz pulse repetition rate, 8 W average power, and 20 ns pulse width shown in figure 3. High Dynamics PIMag® linear XY stages with 100 mm/s speed were used, and the laser beam was directed using the Sino-Galvo SG7210 system. The sample inscribing velocity was set to 100 mm/s. A 15X Objective lens with 0.28 NA from Edmund Optics was used to focus the laser beam.

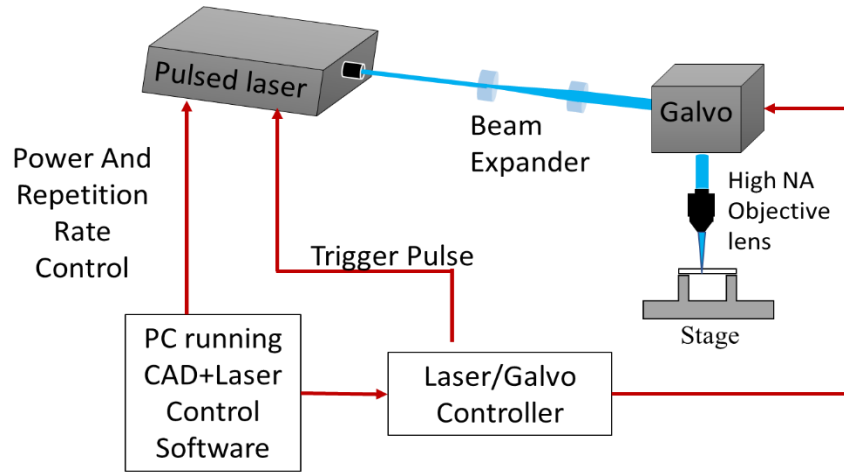


Figure 3: UV nanosecond pulsed laser setup.

2.1.3 Laser-assisted micro-glass vacuum sealing

Glass frit sealing steps involve glass frit and glass plate selection (ensuring both have similar CTE), glass frit deposition, and laser sintering for sealing. In terms of laser processing parameters such as the laser wavelength, laser spot diameter, spot overlap must be appropriately selected.

Glass plates of type Scott B270 with glass transition temperature (T_g) of 542 °C and CTE of $94 \times 10^{-7} / ^\circ\text{C}$ with size ($25 \times 25 \text{ mm}^2$) and 1 mm thickness were used in this study. The glass frit powder without any solvent or binder was optically transparent and was purchased from the AGC company. The frit has a glass transition temperature T_g of 471 °C, CTE of $72 \times 10^{-7} / ^\circ\text{C}$, and an average particle size of 2.2 μm .

The glass frit was made into a paste using isopropyl alcohol (IPA), and a 100 μm thick layer was deposited using a doctor blade method on to bottom glass plate. The top glass was placed onto the glass frit and left at room temperature for 15 min for the IPA to evaporate, as shown in figure 4. The samples were laser sintered on the aluminum block, which acted as a passive heat sink during the process. The laser used was a quasi-continuous wave (QCW) near-infrared laser

of wavelength 1070 nm, 0.1 ms pulse width, and 200 μm spot size. The laser peak power was 1500 W at 100% power. The laser spot scanning was controlled by Galvo with an F-theta lens (SL-1064-112-160Q). To ensure proper melting without additional preheating, laser scanning was done with the fast scan and multiple times following the circumference and traveling to the center as shown in figure 5, and the experimental setup employed in this study is shown in figure 6.

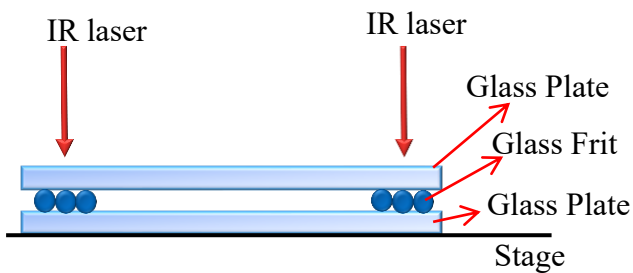


Figure 4: Schematic of the laser glass sealing

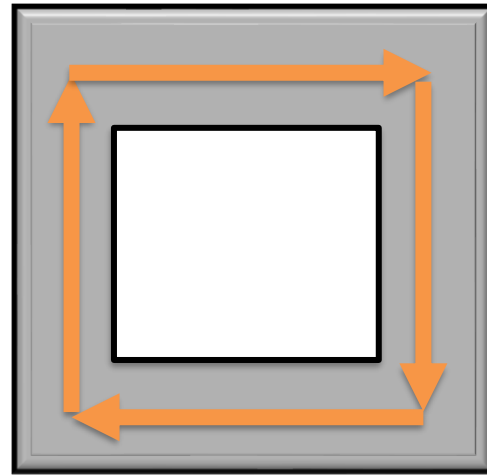


Figure 5: Direction of laser scanning.

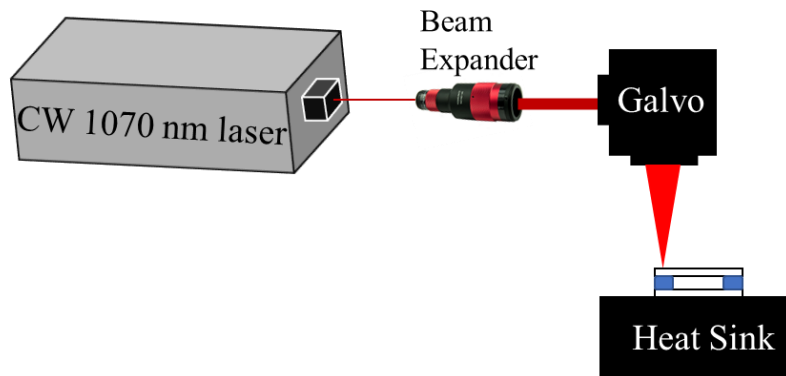


Figure 6: IR laser setup with heatsink.

2.2 Characterization

Newport LBP2-HR-VIS2 beam profiler, S302C thermal power sensor, and 5mW He-Ne, 632 nm wavelength laser, were used to characterize the transmission efficiency and beam profile shown in figure 7. FEI Quanta 650 Scanning electron microscope (SEM) was used to obtain surface morphology. Zemax software was used for ray tracing and beam profile simulations. The optical transmission measurements were done using a Varian Cary 5E UV-Vis-NIR spectrophotometer, and the wavelength sweep was from 300-1200 nm. The glass seal strength was measured using a Nidec force gauge with the setup shown in figure 8.

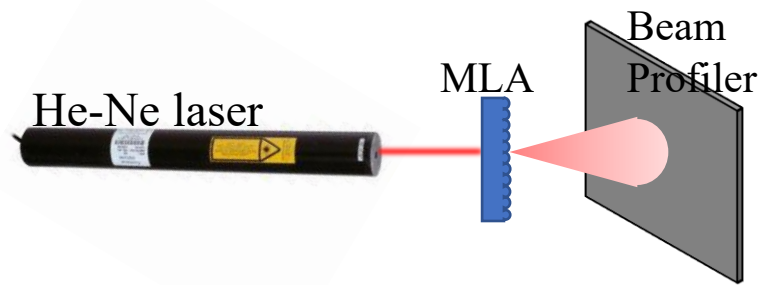


Figure 7: Beam profile measurement setup.

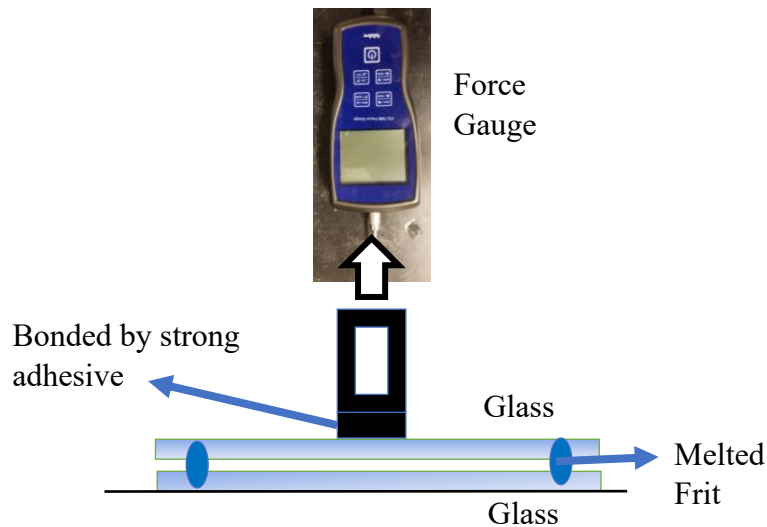


Figure 8: Quantitative adhesion test setup.

3. Results

3.1 Micro lens array properties

3.1.1 Concave lens fabrication by CO₂ laser

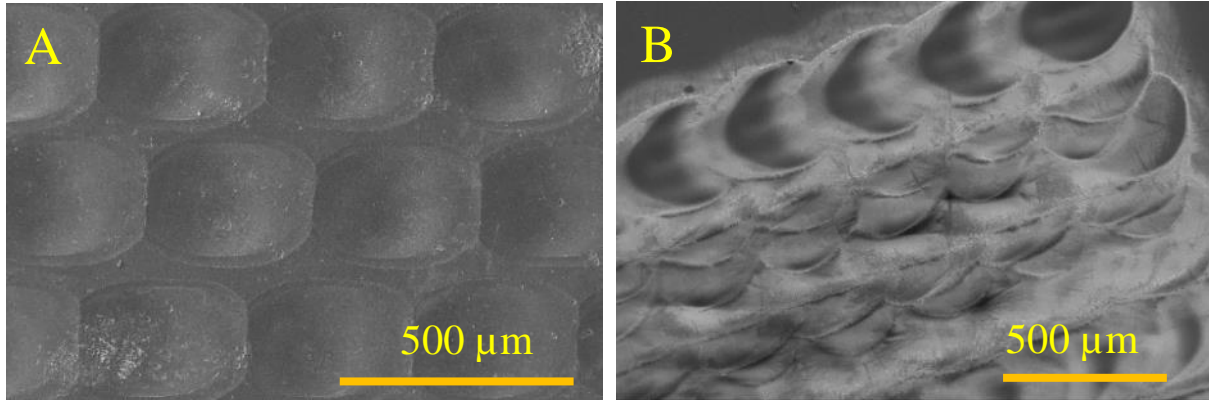


Figure 9: SEM image of concave MLAs using CO₂ laser. (A) Individual concave lenses. (B) Concave lenses with random overlap.

We fabricated concave MLA on fused silica by CO₂ laser irradiation. A 300 μm diameter lens shown in figure 9(A) was fabricated using a laser power density of 43.6 kW/cm² and an exposure time of 0.5 seconds. Due to the periodic nature and small diameter of the micro-lenses, optical diffraction rings were observed in the image of the transmitted beam. To eliminate diffraction effects, the micro lenses were spaced randomly, as shown in figure 9(B). The CO₂ laser-induced melting and solidification reshaped the surface into a concave form. The depth and radius of curvature of the formed concave lens depended upon laser fluence and irradiation time. An increase of time or irradiation fluence produced a higher radius of curvature.

The optical transmission efficiency for the CO₂ laser formed concave MLA was measured as 90.8%. The Zemax software simulations of beam profile at 5 mm, and 10 mm away from the lens are shown in figure 10(A, B). The beam profile for the transmitted light through the CO₂ formed concave lens was measured at 5 mm, and 10 mm distances from the MLA surface, and the

results are shown in figure 10(C, D). As the Gaussian beam passes through the MLA, the beam expands and homogenizes. The measured divergence angle on the X and Y axis was 6.13° and 8.04° , respectively.

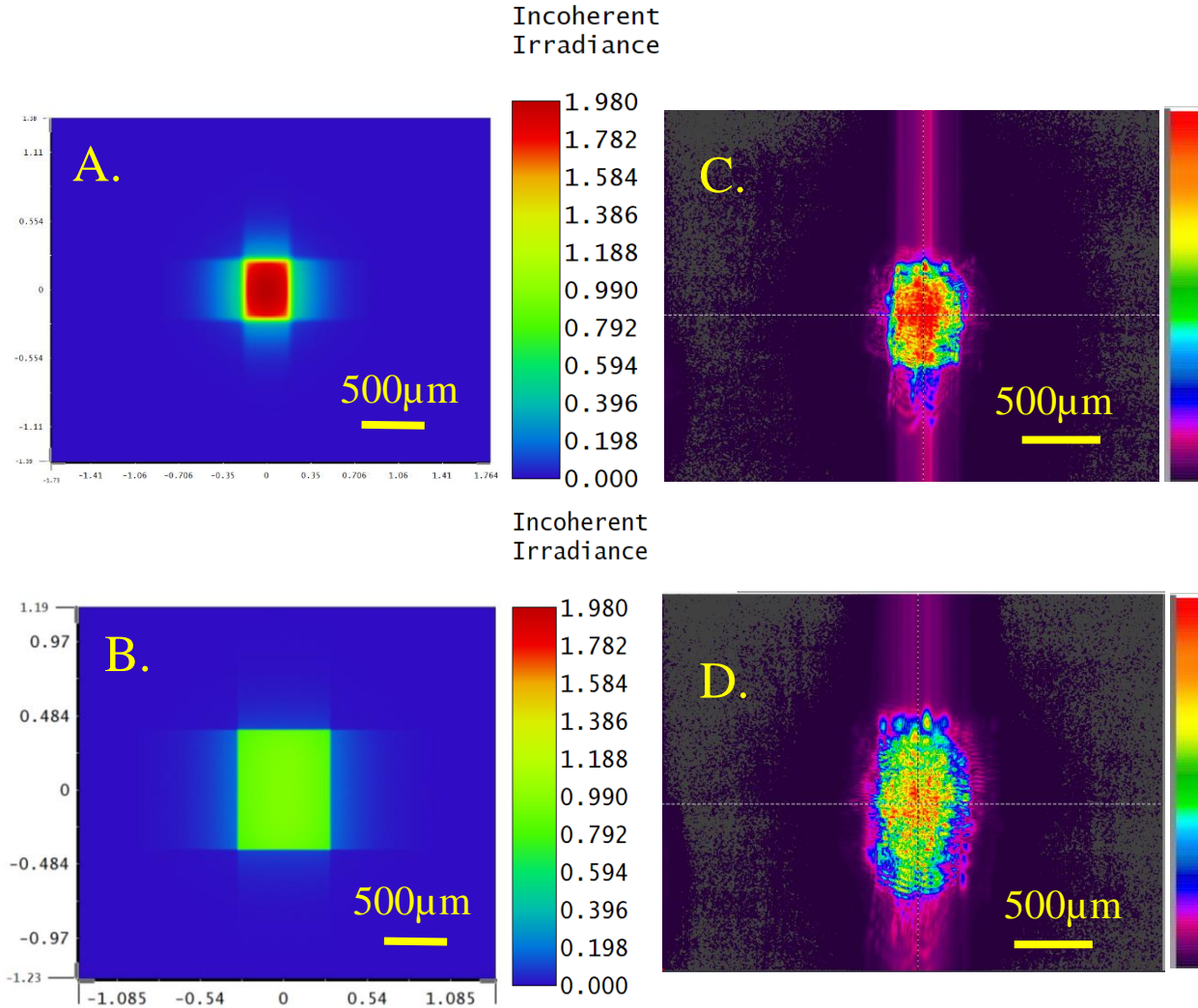


Figure 10: Simulated beam profile of Gaussian beam after passing through the CO₂ fabricated concave MLA at various distances from the lens (A) 5 mm, and (B) 10 mm. Experimentally measured beam profile after passing through the CO₂ concave MLA at various distances from the lens (C) 5 mm, and (D) 10 mm.

3.1.2 Concave lens fabrication by picosecond laser

The concave MLA was fabricated using a picosecond laser. A 25 μm wide diameter lines were fabricated using a laser energy density of 4.66 J/cm^2 shown in figure 11(A). The lenses were spaced randomly to eliminate diffraction effects. The SEM image of these lenses is shown in figure 11(B).

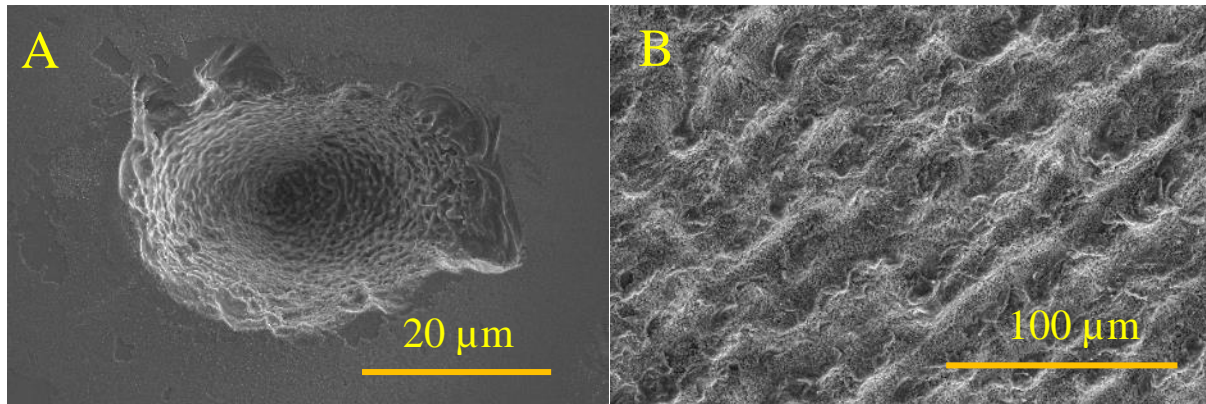


Figure 11: SEM image of concave MLAs using picosecond laser. (A) Individual concave lens. (B) Concave lenses with random overlap.

The optical transmission efficiency for picosecond laser formed concave MLA was measured as 85.2%. The simulations of transmitted beam profiles at various distances from the lens of 5 mm, and 10 mm are shown in figure 12(A, B). The experimentally measured optical beam profile at 5 mm, and 10 mm are from the concave MLA surface are shown in figure 12(C, D). The measured beam divergence angle on the X and Y axis was 11.99° and 15.09°, respectively.

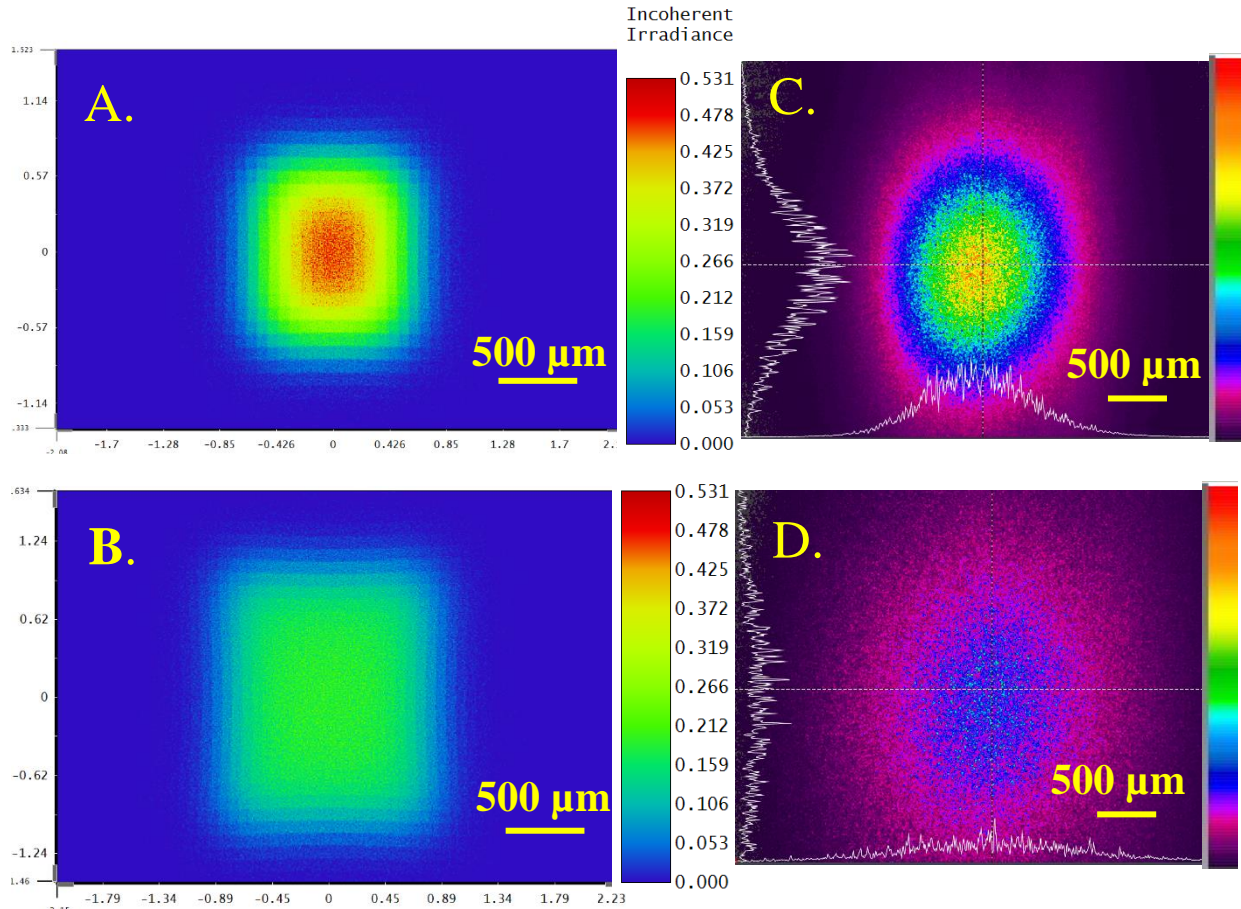


Figure 12: Simulated beam profile of Gaussian beam after passing through the picosecond laser fabricated concave MLA at various distances from the lens (A) 5 mm, and (B) 10 mm. Experimentally measured beam profile after passing through the picosecond laser fabricated concave MLA at various distances from the lens (C) 5 mm, and (D) 10 mm.

3.1.3 Cylindrical lens fabrication by combining picosecond and CO₂ lasers

The cylindrical lens was fabricated by inscribing periodic lines with 50 μm spacing to form vertical structures using the picosecond laser, as shown in figure 13(A). The vertical structures formed by the picosecond laser were remelted to form a cylindrical lens using the CO₂ laser with a power density of 25.2 kW/cm², as shown in figure 13(B).

The transmission efficiency for cylindrical MLA was measured as 86.7%. The simulations of the optical transmitted beam profile at various distances from the lens of 5mm, and 10 mm are

shown in figure 14(A, B). The experimentally measured beam profile of the transmitted beam at various distances from the lens of 5 mm, and 10 mm and are shown in figure 14(C, D). The measured beam divergence angle on the X and Y axis was 5.55° and 11.33° , respectively.

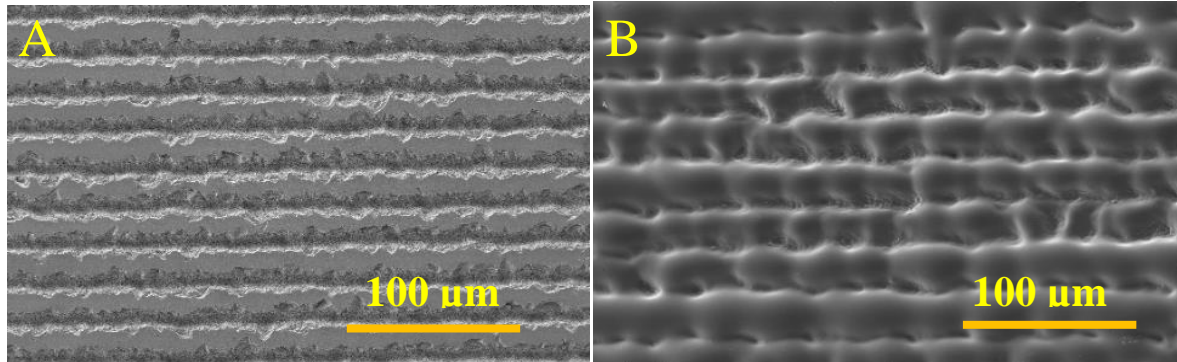


Figure 13: SEM image of (A) picosecond laser micromachined line pattern. (B) cylindrical lenses after CO₂ laser melting.

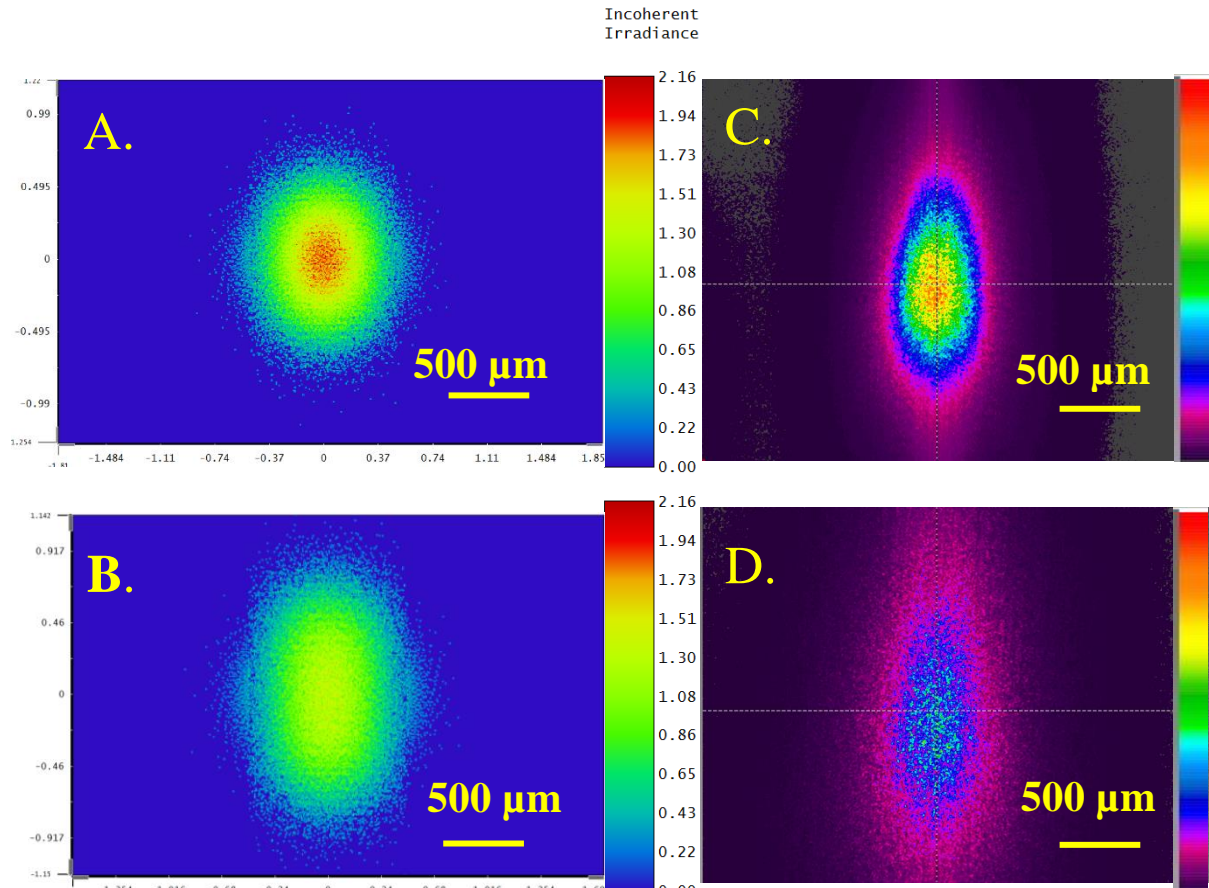


Figure 14: Simulated beam profile of Gaussian beam after passing through the cylindrical MLA at various distances from the lens (A) 5 mm, and (B) 10 mm. Experimentally measured beam profile after passing through the cylindrical MLA at various distances from the lens (C) 5 mm, and (D) 10 mm.

3.1.4 Convex lens fabrication by combining CO₂ and picosecond laser

The convex lens was fabricated by inscribing a perpendicular line array using a picosecond laser to form square structures. The spacing between lines was 50 μm. The pillar structures were remelted using a CO₂ laser with a power density of 25.2 kW/cm² to form convex lenses. The SEM image of the convex MLA is shown in figure 15.

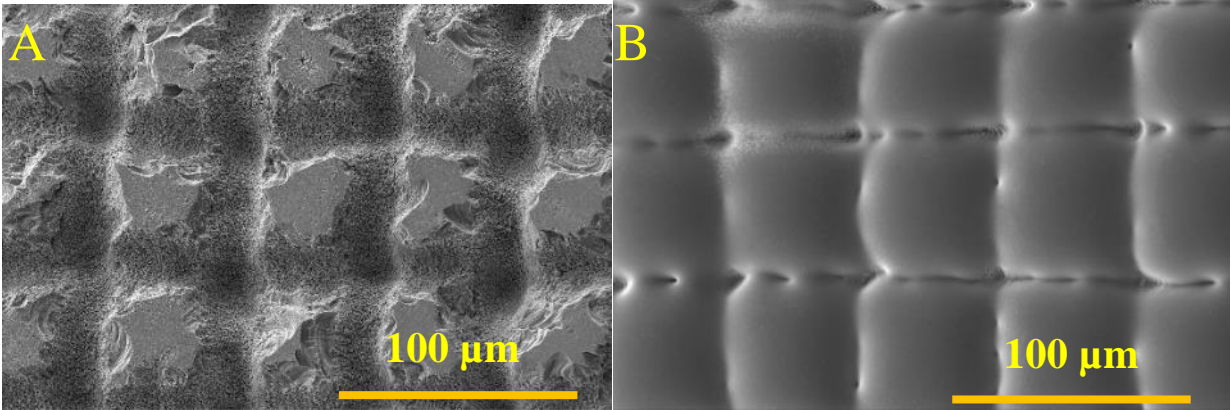


Figure 15: SEM image of (A) picosecond laser micromachined perpendicular line pattern. (B) convex lenses after CO₂ laser melting.

The measured transmission efficiency of convex MLA was 84.3%. The simulations of beam profile after transmission through the lens at various distances from the lens of 5 mm, and 10 mm are shown in figure 16(A, B). The experimentally measured beam profile at various distances from the lens of 5 mm, and 10 mm are shown in figure 16(D, E). The measured beam divergence angle on the X and Y axis was 13.35° and 15.56°, respectively. As the beam is passed through a convex lens, the beam profile transforms into a square flat-top beam, as shown in figure 16(C, F).

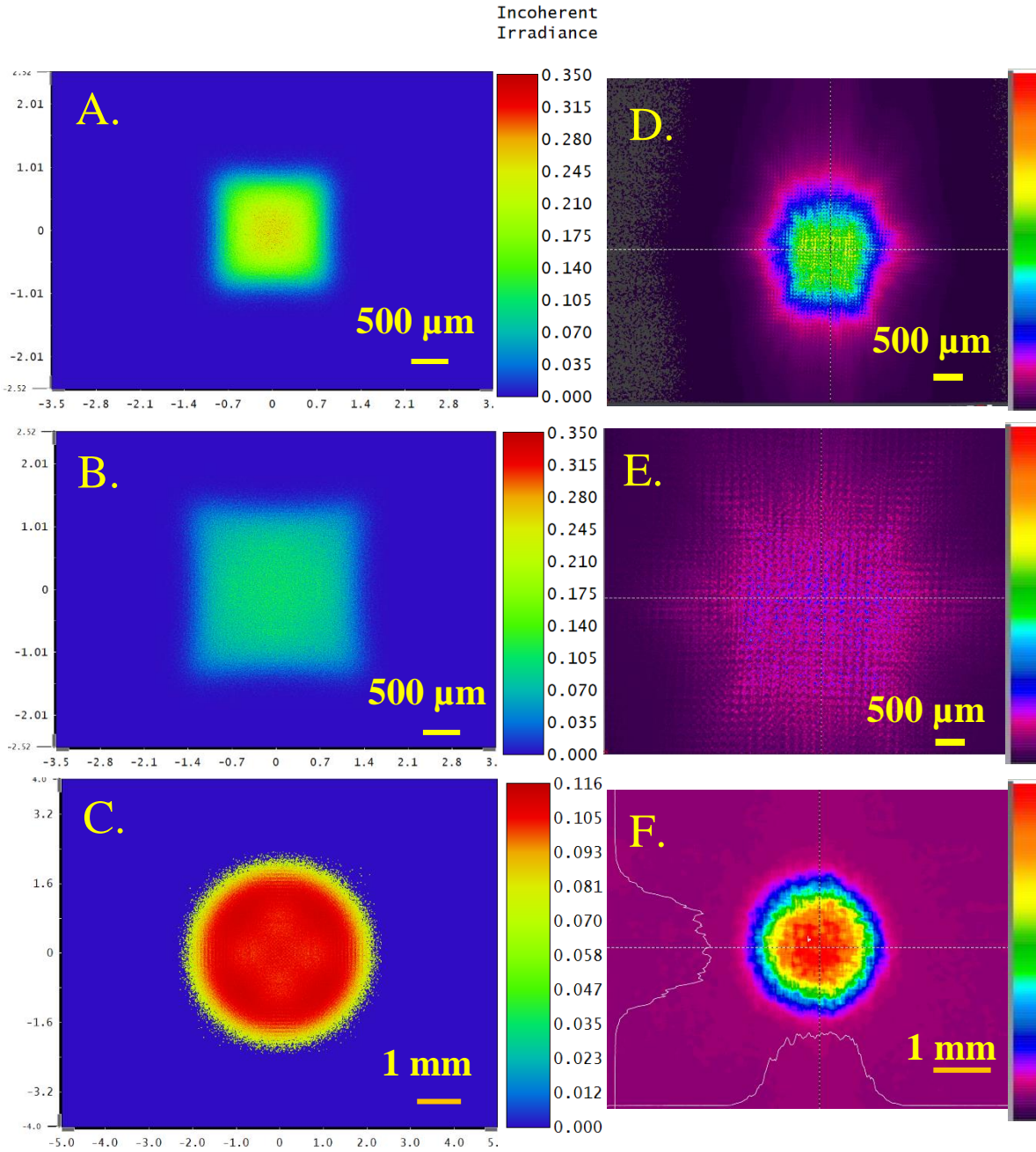


Figure 16: Simulated beam profile of Gaussian beam after passing through the convex MLA at various distances from the lens (A) 5 mm, (B) 10 mm, and (C) flat top beam profile after beam passes through MLA and convex lens. Experimentally measured beam profile after passing through the convex MLA at various distances from the lens (D) 5 mm, (E) 10 mm, (F) flat top beam profile after beam passes through MLA and convex lens.

Table 1. Comparison of lens parameter for various fabrication processes.

Parameter	ps laser fabrication (Concave lens)	CO₂ laser fabrication (Concave lens)	ps+CO₂ laser fabrication (Convex lens)	ps+CO₂ laser fabrication (Cylindrical lens)
μ-lens diameter (μm)	55.94	421.94	63.74	24.39
μ-lens height (μm)	6.14	27.4	6.5	3.1
Measured Focal length (μm)	-145.64	-1796.7	177.49	55.69
Transmission efficiency	85.2 %	90.8 %	84.3 %	86.7 %
Beam divergence (degrees)	X: 11.99 Y: 15.09	X: 6.13 Y: 8.04	X: 13.35 Y: 15.56	X: 5.55 Y: 11.33
Fabrication time for 1-inch MLA	2 min	1 min	4 min	4 min

3.2 Laser micro patterning of sapphire

3.2.1 Fabrication of Diffraction gratings

Diffraction gratings patterns were micromachined on sapphire using nanosecond laser passing through 0.28 NA objective lens. Diffraction angles can be calculated from,

$$d \cdot \sin\Theta = m\lambda$$

where, d is the line spacing, m is the order of maxima, λ is the wavelength of the incident light and Θ is the diffraction angle.

Figure 17 shows patterned lines when the laser is focused on the top surface. The linewidth measured was $4.47\ \mu\text{m}$, and the line spacing was $6.38\ \mu\text{m}$. Figure 18 shows the diffraction beam pattern as He-Ne laser beam passes through the grating. The calculated and measured first order diffraction angles were 3.12° and 2.26° , respectively.

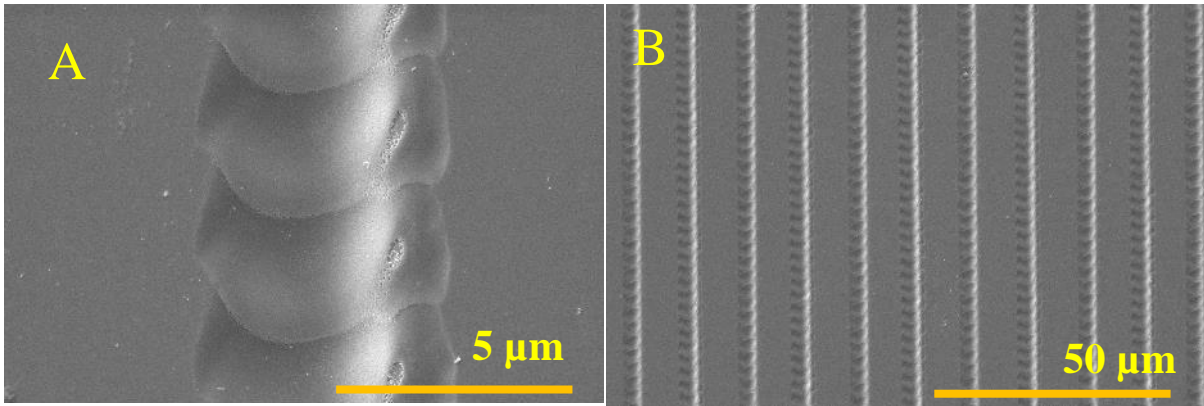


Figure 17: SEM image of diffraction grating pattern when laser beam was focused on the top surface.

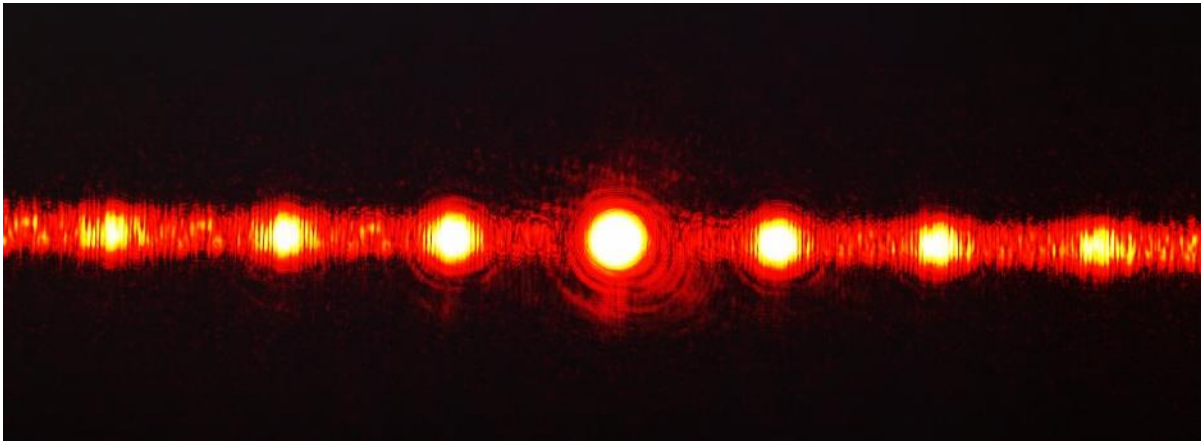


Figure 18: Diffraction grating beam profile for pattern fabrication on the top surface.

Figure 19 shows patterned lines as the laser beam is focused on the bottom surface. The linewidth measured was $4.4\ \mu\text{m}$, and the line spacing was $5.26\ \mu\text{m}$. Figure 20 shows the diffraction beam pattern as the He-Ne beam passes through the grating. The calculated and measured first order diffraction angles were 3.7° and 3.4° , respectively.

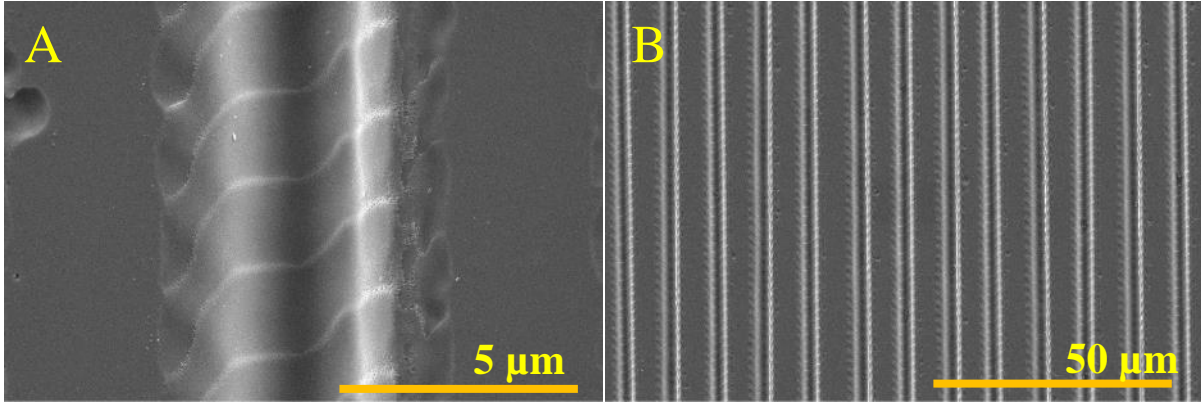


Figure 19: SEM image of diffraction grating pattern when laser beam was focused on the bottom surface.

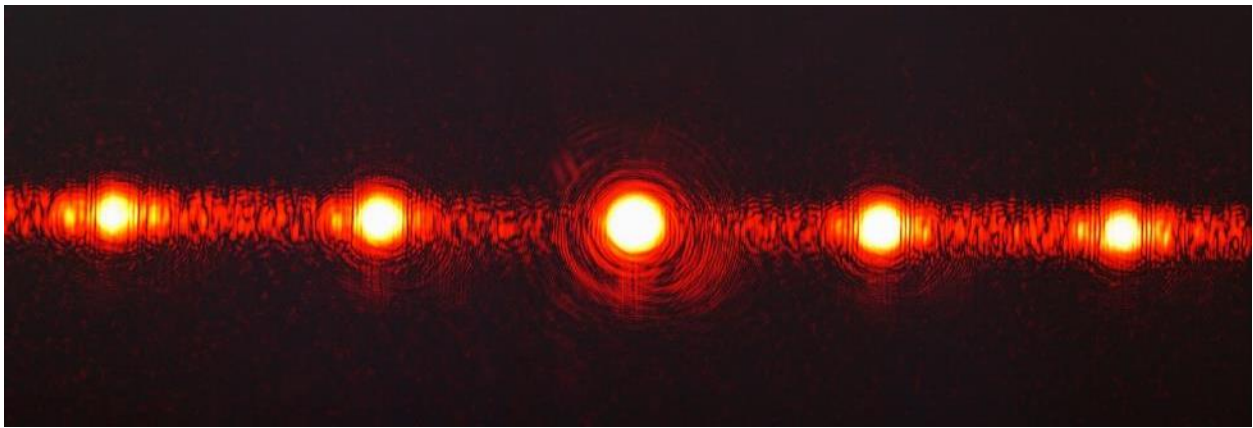


Figure 20: Diffraction grating beam profile for pattern fabrication on the bottom surface.

3.2.2 Fabrication of photon sieve

The photon sieve was patterned on sapphire using nanosecond laser passing through 0.28 NA objective lens. Figure 21 shows SEM image of the photon sieve. Figure 22 (A) shows the beam profile of He-Ne laser and figure 22(B) shows beam profile at 77 mm after passing through the photon sieve showing the focused beam.

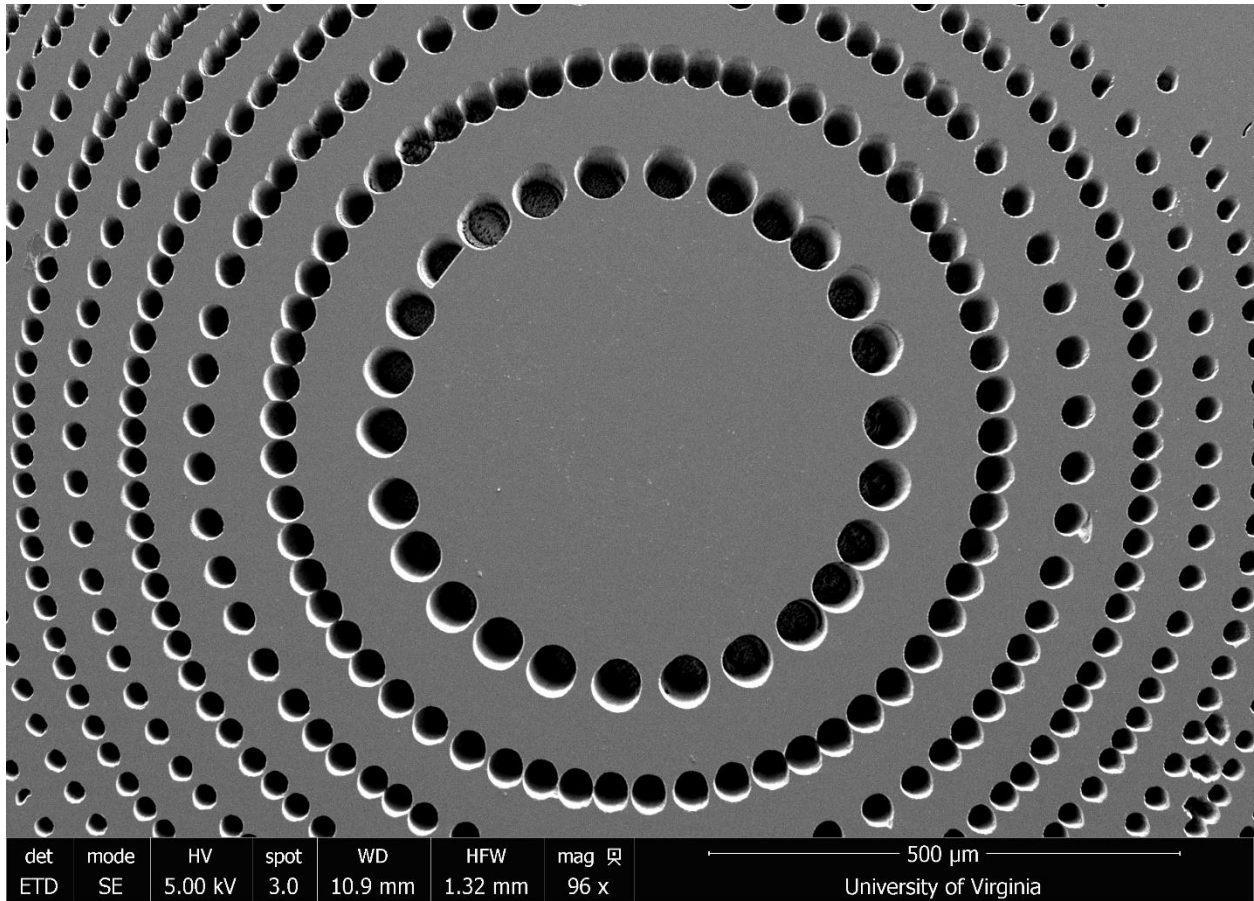


Figure 21: SEM image of photon sieve on sapphire substrate.

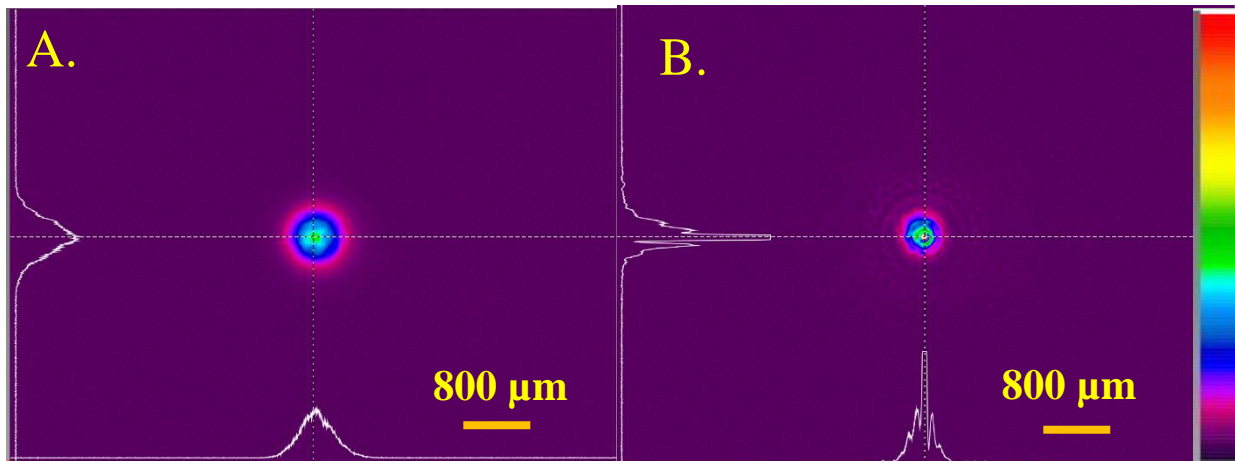


Figure 22: Experimentally measured beam profile (A) He-Ne laser beam profile, (B) beam profile after passing through the photon sieve, 77 mm from the photon sieve surface.

The 632nm wavelength CW laser beam FWHM was 425 μm . The resulting focal point FWHM and focusing efficiency were 112 μm and 24.5%, respectively.

3.3 Micro scale laser-assisted glass vacuum sealing

Two sintering methods were studied with different laser processing parameters, and the results were compared with the conventional furnace process. Laser parameters with 200 μm spot size were set with 50 mm/s scan speed with 0.05 mm line spacing (TEST A). The second run was done with a laser spot size of 200 μm , a scan speed of 200 mm/s, and a line overlap of 0.01 mm (TEST B); this increased the spot overlap between lines.

Conventional glass sealing was done in a furnace, and the temperature cycle used is shown in figure 23. A 100 μm thick glass frit layer was deposited using the doctor blade method onto a glass plate, and the temperature was raised to 250 $^{\circ}\text{C}$ and held for 1 hour to remove solvent from the frit. The temperature was further raised to the transition temperature of the glass frit to 500 $^{\circ}\text{C}$ and held for 5 hours, and finally, it was cooled at a rate of 10 $^{\circ}\text{C}/\text{min}$.

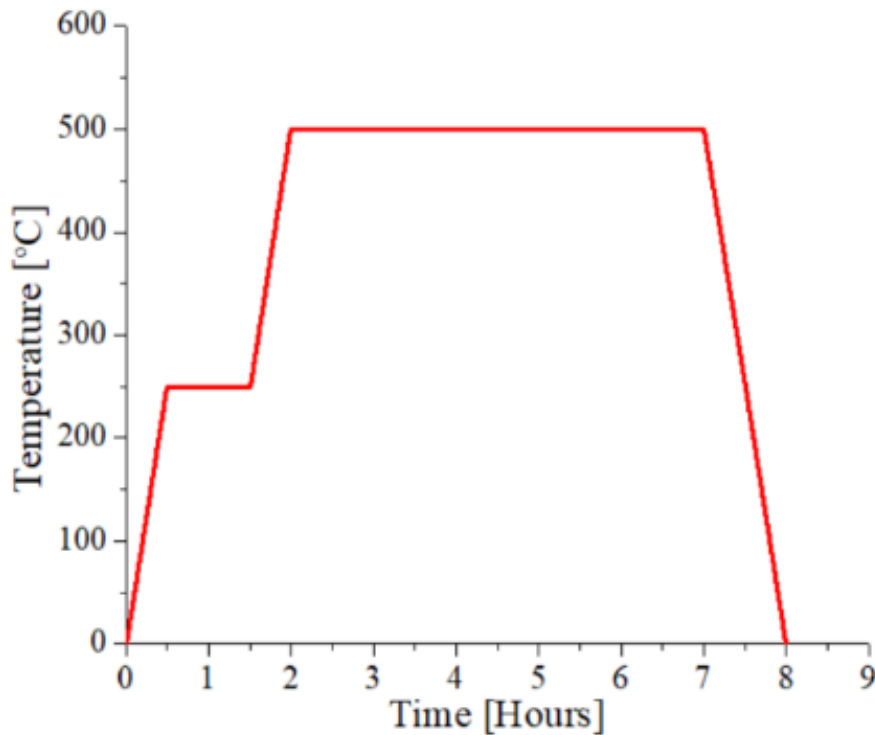


Figure 23: Temperature cycle for glass furnace melting.

Figure 24 shows the optical transmission measurements for TEST A and TEST B, along with the sample images. The reflection and scattering losses from glass to melted frit led to lower transmission values. TEST A has 10 % transparency in the visible region due to incomplete overlap between laser lines. TEST B has higher transmission 24 %, due to higher laser spot overlap ensuring complete frit melting. Figure 25 (a, b) show an optical image of the furnace melted frit and of TEST B sample, respectively. The trapped air pockets within the frit melt can be seen, which caused light scattering and hence the lowering of the optical transmission. The line overlap does not appear to be sufficient.

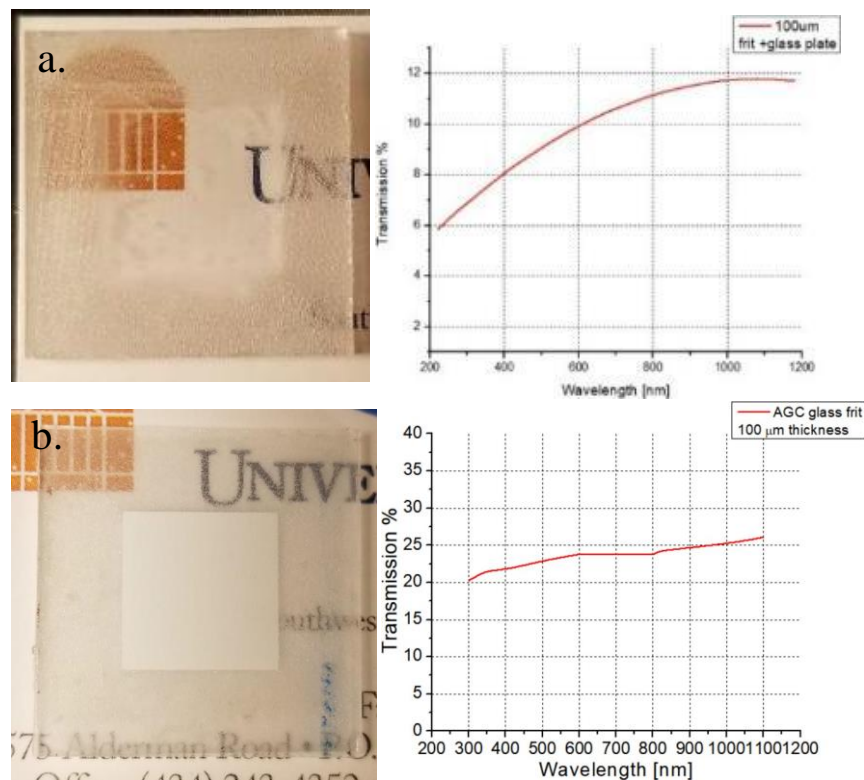


Figure 24: Optical Transmission measurement for (a)TEST A and (b)TEST b.

The glass seal strength was measured for samples with laser sealing and furnace methods, and the results are shown in figure 26. The seal strength between the two tests is close to 25 kN/m². At the same time, the seal strength by furnace was much higher at 78 MN/m². This preliminary

study demonstrates the transparent glass frit sealing using laser melting process to control thermal stress during the melting process, and crack-free samples were obtained.

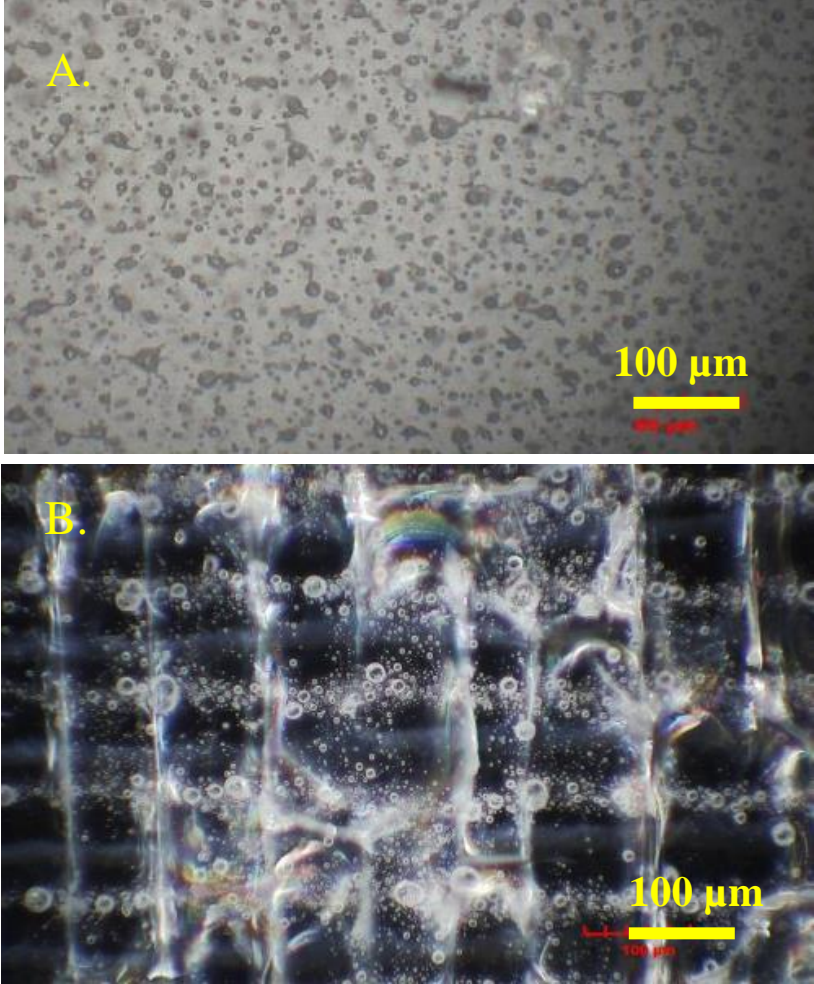


Figure 25: Optical image of laser melted glass frit for (A) furnace melted glass frit and (B) TEST B sample.

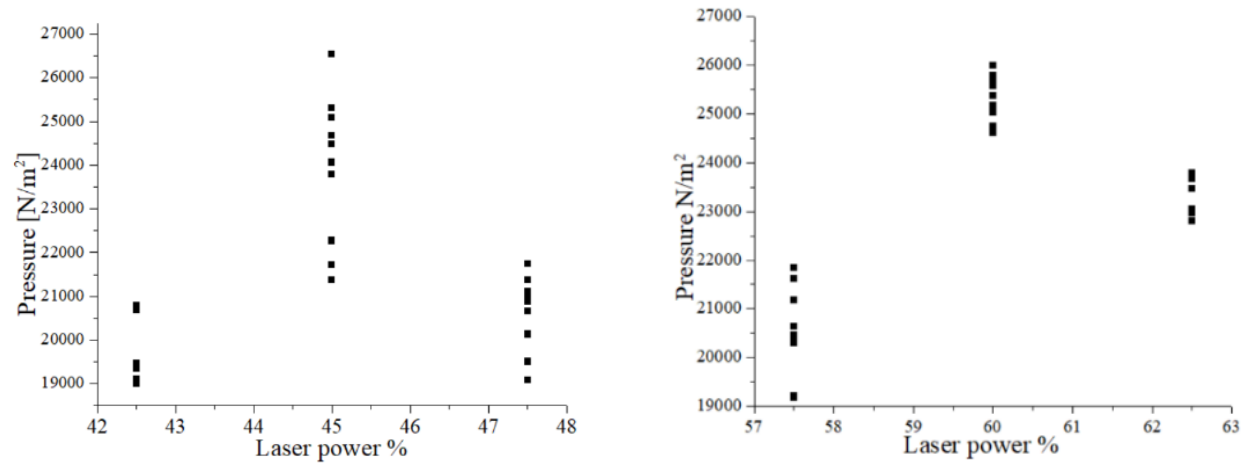


Figure 26: Seal strength measurements for (a)TEST A and (b)TEST B.

4. Conclusions and Future Work

4.1 Conclusions

Firstly, we successfully fabricated concave MLA by picosecond laser ablation and also by CO₂ laser as well as convex MLA by combining ps micromachining with CO₂ laser-induced melting process. The fabricated MLAs had high light transmission efficiency of >84%. We simulated the transmitted light beam profile for the MLAs at different distances from the lens using Zemax software. A good agreement between the simulations and measurements was observed. The laser fabrication process is faster, and can generate large area MLAs. The laser process can be applied to other optical materials like sapphire, silicon, and Zinc selenide for the fabrication of micro lenses.

Secondly, we successfully fabricated diffraction gratings in sapphire by nanosecond pulsed laser ablation and measured the beam profile. A good agreement was observed between the calculated and measured diffraction angle for gratings fabricated on top and bottom surfaces. We also fabricated a photon sieve designed for 632.8 nm wavelength and studied the beam profile at the focal point.

Finally, we have demonstrated laser sealing of glass plates using localized laser melting of optically transparent and low-melting temperature (471 °C) glass frit without heating of glass plates. The glass plate bond strength value of 25000 N/m² was achieved, and optical transmission was 24 %.

4.2 Future Work

4.2.1 Micro-lens

Although the MLAs have high transmission efficiencies, they can be further improved by eliminating defects at the lens corners. Reducing the lens sizes and patterning a Fresnel lens can provide lenses with much less radius of curvature and improve optical transmission efficiencies.

4.2.2 Micro-patterning

The current laser beam size can be used to fabricate optical devices in the IR range. Using a higher NA objective, the gratings for the visible wavelengths can be realized. Using current software, devices can be designed for visible and infrared spectrum. we can model and fabricate photonic devices.

4.2.3 Micro-sealing

The lower optical transmission and bond strength can be improved by using lower glass transition temperature (T_g) and transparent frit as from the results, we can observe better optical and physical properties when the frit has more time to melt and flow before solidification. Lower temperature requires less laser power to melt and eliminate any decomposition of the oxides and lowering air pockets in the seal. Reducing the frit size through the ball milling process can also have better results as smaller particles can be more densely packed, reducing air pockets.

Appendix: Publications

A. Fabrication and Comparative Study of Micro-Lenses Obtained by Solid State Picosecond and CW CO₂ Laser.

Narayana Raju Gottumukkala¹, Caleb Barnes, and Mool C. Gupta¹

¹Department of Electrical and Computer Engineering, University of Virginia, Charlottesville, VA 22904, USA

Email: mgupta@virginia.edu

Abstract

We report on fabricating plano-convex and cylindrical micro-lens array on fused silica by patterned micro-machining using a 355 nm wavelength picosecond pulsed laser and reshaping using a CW CO₂ laser. We also fabricate plano-concave micro-lens array using picosecond pulsed laser and CW CO₂ laser. We report the results on the surface morphology, optical transmission efficiency, laser beam profile of transmitted light passing through the micro-lens, and transforming arbitrary laser beam shape into a flat-top beam. Furthermore, we compare results with commercially available micro-lenses fabricated by lithography process and discuss the advantage of our fast and repeatable technique. We have also performed a comparative performance study of plano-concave micro-lenses obtained by individual picosecond and CO₂ lasers.

Manuscript under preparation for submission to Journal of Applied Optics

B. Fabrication and Optical Analysis of Diffractive Optical Elements by Nanosecond Pulsed Laser

Narayana Raju Gottumukkala¹, and Mool C. Gupta¹

¹Department of Electrical and Computer Engineering, University of Virginia, Charlottesville,

VA 22904, USA

Email: mgupta@virginia.edu

Abstract

We demonstrate micro machining of sapphire for diffractive optical elements fabrication using a 355 nm wavelength nanosecond pulsed laser. We report results on diffraction gratings using laser processing on sapphire producing 50% duty cycle with 4.6 μm line widths, respectively. We also demonstrate the design, fabrication and characterization of photon sieve with 24.5% transmission efficiency.

Manuscript under preparation for submission to Journal of Applied Optics

C. Glass Sealing by CW Laser Melting of Low Temperature Frit

Narayana Raju Gottumukkala¹, and Mool C. Gupta¹

¹Department of Electrical and Computer Engineering, University of Virginia, Charlottesville,
VA 22904, USA

Email: mgupta@virginia.edu

Abstract

Experimental results are presented on glass sealing by a continuous wave 1070 nm wavelength laser at room temperature. The seal was accomplished by using laser radiation to pass through top glass plate and melting the glass frit deposited on the bottom glass plate. The optical transmission of the sealed glass plate was 23.5 %. The bond strength between the glass plates was measured as 25000 N/m².

Manuscript under preparation for submission to Journal of Applied Optics

References

- [1] F. Chen *et al.*, “Maskless fabrication of concave microlens arrays on silica glasses by a femtosecond-laser-enhanced local wet etching method,” *Opt. Express*, vol. 18, no. 19, pp. 20334–20343, 2010, doi: 10.1364/OE.18.020334.
- [2] Y. Hu *et al.*, “Cost-efficient and flexible fabrication of rectangular-shaped microlens arrays with controllable aspect ratio and spherical morphology,” *Appl. Surf. Sci.*, vol. 292, pp. 285–290, 2014, doi: <https://doi.org/10.1016/j.apsusc.2013.11.132>.
- [3] X.-W. Cao *et al.*, “Single-pulse writing of a concave microlens array,” *Opt. Lett.*, vol. 43, no. 4, pp. 831–834, 2018, doi: 10.1364/OL.43.000831.
- [4] J. Zhu, M. Li, J. Qiu, and H. Ye, “Fabrication of high fill-factor aspheric microlens array by dose-modulated lithography and low temperature thermal reflow,” *Microsyst. Technol.*, vol. 25, no. 4, pp. 1235–1241, 2019, doi: 10.1007/s00542-018-4226-2.
- [5] X. Zhu, L. Zhu, H. Chen, M. Yang, and W. Zhang, “Fabrication of multi-scale micro-lens arrays on hydrophobic surfaces using a drop-on-demand droplet generator,” *Opt. Laser Technol.*, vol. 66, Feb. 2015, doi: 10.1016/j.optlastec.2014.09.002.
- [6] C. R. Forest, M. A. Saez, and I. W. Hunter, “Microforging technique for rapid, low-cost fabrication of lens array molds,” *Appl. Opt.*, vol. 46, no. 36, pp. 8668–8673, 2007, doi: 10.1364/AO.46.008668.
- [7] H. Zuo, D.-Y. Choi, X. Gai, B. Luther-Davies, and B. Zhang, “CMOS compatible fabrication of micro, nano convex silicon lens arrays by conformal chemical vapor deposition,” *Opt. Express*, vol. 25, no. 4, pp. 3069–3076, 2017, doi: 10.1364/OE.25.003069.
- [8] S. Yang *et al.*, “CO₂ laser thermal reflow shaped convex glass microlens array after Bessel picosecond laser inscribing and hydrofluoric acid processing,” *Appl. Opt.*, vol. 59, no. 4, pp. 1099–1104, 2020, doi: 10.1364/AO.383189.
- [9] I.-B. Sohn *et al.*, “Formation of plano-convex micro-lens array in fused silica glass using CO₂ laser assisted reshaping technique,” *J. Korean Phys. Soc.*, vol. 69, May 2016, doi: 10.3938/jkps.69.335.
- [10] T. Schmidt and D. Conrad, “Micro lens arrays made by CO₂-laser radiation,” in *Proc.SPIE*, Jul. 2020, vol. 11478, doi: 10.1117/12.2566485.
- [11] S. Schwarz, B. Götzendorfer, S. Rung, C. Esen, and R. Hellmann, “Compact Beam Homogenizer Module with Laser-Fabricated Lens-Arrays,” *Applied Sciences*, vol. 11, no. 3. 2021, doi: 10.3390/app11031018.
- [12] S. Büttner, M. Pfeifer, and S. Weissmantel, “Manufacturing of Cylindrical Micro Lenses and Micro Lens Arrays in Fused Silica and Borosilicate Glass using F2-Laser Microstructuring,” 2019.
- [13] G. Andersen, “Membrane photon sieve telescopes,” *Appl. Opt.*, vol. 49, no. 33, pp. 6391–6394, 2010, doi: 10.1364/AO.49.006391.
- [14] X. Zhao, F. Xu, J. Hu, and C. Wang, “Broadband photon sieves imaging with wavefront

- coding,” *Opt. Express*, vol. 23, no. 13, pp. 16812–16822, 2015, doi: 10.1364/OE.23.016812.
- [15] R. Janeiro, R. Flores, P. Dahal, and J. Viegas, “Fabrication of a phase photon sieve on an optical fiber tip by focused ion beam nanomachining for improved fiber to silicon photonics waveguide light coupling,” *Opt. Express*, vol. 24, p. 11611, May 2016, doi: 10.1364/OE.24.011611.
- [16] K.-H. Brenner and F. Sauer, “Diffractive–reflective optical interconnects,” *Appl. Opt.*, vol. 27, no. 20, pp. 4251–4254, 1988, doi: 10.1364/AO.27.004251.
- [17] N. W. Parker, A. D. Brodie, and J. H. McCoy, “High-throughput NGL electron-beam direct-write lithography system,” in *Proc.SPIE*, Jul. 2000, vol. 3997, doi: 10.1117/12.390042.
- [18] X. Zhou, X. Liu, D. Zhang, Z. Shen, and W. Liu, “Balling phenomena in selective laser melted tungsten,” *J. Mater. Process. Technol.*, vol. 222, pp. 33–42, 2015, doi: <https://doi.org/10.1016/j.jmatprotec.2015.02.032>.
- [19] P. O. Caffrey, B. K. Nayak, and M. C. Gupta, “Ultrafast laser-induced microstructure/nanostructure replication and optical properties,” *Appl. Opt.*, vol. 51, no. 5, pp. 604–609, 2012, doi: 10.1364/AO.51.000604.
- [20] P. P. Pronko, S. K. Dutta, J. Squier, J. V Rudd, D. Du, and G. Mourou, “Machining of sub-micron holes using a femtosecond laser at 800 nm,” *Opt. Commun.*, vol. 114, no. 1, pp. 106–110, 1995, doi: [https://doi.org/10.1016/0030-4018\(94\)00585-1](https://doi.org/10.1016/0030-4018(94)00585-1).
- [21] L. Kipp *et al.*, “Sharper images by focusing soft X-rays with photon sieves,” *Nature*, vol. 414, no. 6860, pp. 184–188, 2001, doi: 10.1038/35102526.
- [22] X. Zhao *et al.*, “Ultra-broadband achromatic imaging with diffractive photon sieves,” *Sci. Rep.*, vol. 6, no. 1, p. 28319, 2016, doi: 10.1038/srep28319.
- [23] S. Emami, J. Martins, L. Andrade, J. Mendes, and A. Mendes, “Low temperature hermetic laser-assisted glass frit encapsulation of soda-lime glass substrates,” *Opt. Lasers Eng.*, vol. 96, pp. 107–116, 2017, doi: <https://doi.org/10.1016/j.optlaseng.2017.04.006>.
- [24] H. Kind, E. Gehlen, M. Aden, A. Olowinsky, and A. Gillner, “Laser Glass Frit Sealing for Encapsulation of Vacuum Insulation Glasses,” *Phys. Procedia*, vol. 56, pp. 673–680, 2014, doi: <https://doi.org/10.1016/j.phpro.2014.08.075>.
- [25] F. Ribeiro, J. Maçaira, R. Cruz, J. Gabriel, L. Andrade, and A. Mendes, “Laser assisted glass frit sealing of dye-sensitized solar cells,” *Sol. Energy Mater. Sol. Cells*, vol. 96, pp. 43–49, 2012, doi: <https://doi.org/10.1016/j.solmat.2011.09.009>.
- [26] C. Dresbach, A. Krombholz, M. Ebert, and J. Bagdahn, “Mechanical properties of glass frit bonded micro packages,” *Microsyst. Technol.*, vol. 12, no. 5, pp. 473–480, 2006, doi: 10.1007/s00542-005-0031-9.
- [27] N. Lorenz, S. Millar, M. Desmulliez, and D. P. Hand, “Hermetic glass frit packaging in air and vacuum with localized laser joining,” *J. Micromechanics Microengineering*, vol. 21, no. 4, p. 45039, Mar. 2011, doi: 10.1088/0960-1317/21/4/045039.

- [28] S. Logunov, S. Marjanovic, and J. Balakrishnan, “Laser Assisted Frit Sealing for High Thermal Expansion Glasses,” *J. Laser Micro Nanoeng.*, vol. 7, pp. 326–333, 2012.
- [29] D. K. Ivanou, R. Santos, J. Maçaira, L. Andrade, and A. Mendes, “Laser assisted glass frit sealing for production large area DSCs panels,” *Sol. Energy*, vol. 135, pp. 674–681, 2016, doi: <https://doi.org/10.1016/j.solener.2016.06.043>.